

Enabling the 3D Printing of Metal Components in μ -Gravity

Andrea Zocca,* Jörg Luchtenborg, Thomas Mühler, Janka Wilbig, Gunther Mohr, Thomas Villatte, Fabien Léonard, Gert Nolze, Marc Sparenberg, Jörg Melcher, Kai Hilgenberg, and Jens Günster

As humanity contemplates manned missions to Mars, strategies need to be developed for the design and operation of hospitable environments to safely work in space for years. The supply of spare parts for repair and replacement of lost equipment will be one key need, but in-space manufacturing remains the only option for a timely supply. With high flexibility in design and the ability to manufacture ready-to-use components directly from a computer-aided model, additive manufacturing (AM) technologies appear extremely attractive. For the manufacturing of metal parts, laser-beam melting is the most widely used AM process. However, the handling of metal powders in the absence of gravity is one prerequisite for its successful application in space. A gas flow throughout the powder bed is successfully applied to compensate for missing gravitational forces in microgravity experiments. This so-called gas-flow-assisted powder deposition is based on a porous building platform acting as a filter for the fixation of metal particles in a gas flow driven by a pressure difference maintained by a vacuum pump.

matter. The value of spare parts supply for the ISS has been estimated by NASA exceeding 1.2 billion \$ over the course of the period 2008–2017 with \approx 300 million \$ accounting for batteries.^[1]

The ISS receives regular shipments, which include also replenishment of the spare parts stock. Still, it is not possible to have every spare part and tool available at any time, due to unforeseen breakdowns, lost tools and not lastly failure of scheduled launches from Earth. Between 2014 and 2015, three shipments failed (Orbital Sciences' private Antares rocket in October 2014; Russia's Progress 59 cargo in May 2015; SpaceX's Falcon 9 rocket in June 2015) before on 5th of July the resupply mission Russia's Progress 60 cargo finally reached the ISS.^[2] Even losing a tool in

the station or during a spacewalk may be problematic for astronauts and mission.^[3] Despite careful tracking, in average roughly 2% of all spare parts in the ISS, summing up to about 2000 components, are at any time lost.

A valuable alternative to resupply space missions is the ability to manufacture objects of any kind directly in space. Given the fact that most standard manufacturing technologies require dedicated tooling, it appears logical to develop additive manufacturing (AM) technologies which can function in microgravity (μ -g) conditions. The vision is, having a "virtual tool" box including all possible spare parts as a model and 3D printing them on demand directly in space. Special parts may even be designed on Earth and their 3D models sent to be 3D printed instead of shipping the object. There is a clear advantage in sending information over sending physical components, because the information can be generated in space or on ground as a reaction to individual incidents or occasions hardly foreseeable in long space missions. Certainly, material and equipment for space manufacturing needs to be on board at launch and carried along with the mission, but still the weight to be carried will be significantly less than the sum of all possible spare parts plus the striking advantage of a timely supply.

Considering future human exploration of the Moon or of Mars, it is even clearer that AM in space becomes a necessity. As the function of their distance to Earth, **Figure 1** compares the respective times needed to reach the ISS, Moon, and Mars by sending a physical object or an information. Obviously, sending resupplying missions to Mars will not be an option and "in-space manufacturing" (ISM) is required to react to part

1. Introduction

1.1. Motivations for Additive Manufacturing in Space


Ordering a spare part on Earth or needing a spare part on the International Space Station (ISS) is a completely different

Dr. A. Zocca, J. Luchtenborg, J. Wilbig, G. Mohr, Dr. F. Léonard, Prof. G. Nolze, Prof. K. Hilgenberg, Prof. J. Günster
Bundesanstalt für Materialforschung und -prüfung (BAM)
Unter den Eichen 87, 12205 Berlin, Germany
E-mail: andrea.zocca@bam.de

Dr. T. Mühler, Prof. J. Günster
Technical University Clausthal
LaserAnwendungsCentrum
Arnold-Sommerfeld-Straße 6, Clausthal-Zellerfeld 38678, Germany

T. Villatte
Novespace
29 Rue Marcel Issartier, 33700 Mérignac, France

Dr. M. Sparenberg, Prof. J. Melcher
Deutsches Zentrum für Luft- und Raumfahrt (DLR)
Lilienthalplatz 7, 38108 Braunschweig, Germany

 The ORCID identification number(s) for the author(s) of this article can be found under <https://doi.org/10.1002/admt.201900506>.

© 2019 The Authors. Published by WILEY-VCH Verlag GmbH & Co. KGaA, Weinheim. This is an open access article under the terms of the Creative Commons Attribution-NonCommercial-NoDerivs License, which permits use and distribution in any medium, provided the original work is properly cited, the use is non-commercial and no modifications or adaptations are made.

DOI: 10.1002/admt.201900506

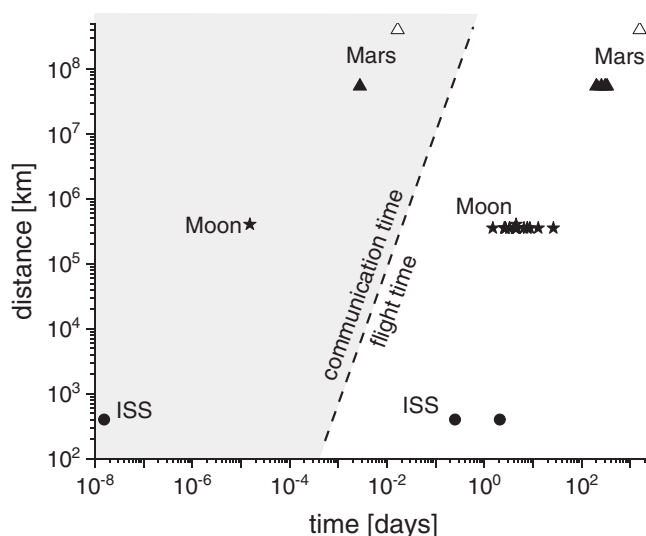


Figure 1. Time needed to reach the ISS, Moon, and Mars as function of their distance to Earth. The values for the required travel times to reach a respective object are based on literature values for different flight trajectories and maneuvers. The Earth–Moon distance considered is at the perigee; for the Earth–Mars distance, filled symbols show the average minimum distance, which is reached every ≈ 26 months. Open symbols show the maximum distance Earth–Mars and hypothetical flight time, although it is to be expected that flight missions are and will be feasible only when Mars is close to its minimum distance.

failures, accidents involving loss or damage of parts or simply demanding special parts not in stock on board of the spacecraft.

The aim of this work is to develop a technology able to fabricate metal components in space, in a size range from 1 to 500 mm. Even larger structures could be assembled and, thus, this approach would cover the size range of most spare parts aboard a spacecraft. A considerable number of spare parts in the ISS, approx. 17% of the total, is made of metallic materials, according to the “Problem Resolution and Corresponding Action” database maintained by NASA on the ISS.

Powder bed fusion, and in particular laser beam melting (LBM), is the AM technology of choice to commercially produce ready to use high-performance metallic parts in the required size range. An extensive review of LBM compared to other AM technologies applied to metal alloys has been written by DebRoy et al.^[4] In LBM, thin layers of a flowable powder are deposited on top of each other. In each layer, the cross-section of the object to be produced is inscribed by selectively melting and fusing the metal powder. For this purpose, a focused laser beam is scanned over the entire area of the respective cross-section. LBM has attracted the interest of industries in different fields, such as automotive, aerospace, tool manufacturing, medical devices, and others. The selection of LBM as a process for fabricating aerospace components was primarily based on the weight ratio between the raw material required for machining a component and the weight of the component itself. For conventional fabrication technologies, this “buy-to-fly” ratio can be as high as 15–20 for flying components, adding a lot of cost to the component for material and machining. LBM enables “buy-to-fly” ratios of nearly 1, because of its ability of building up a part from a powdery material with almost no waste. Bearing in

mind the flexibility of producing parts with almost any shape and the ability to provide ready to use parts in one process step, LBM appears extremely attractive for ISM. Moreover, a wide range of metallic feedstocks, such as titanium-, aluminum-, nickel-based alloys and stainless steels, can be processed.

1.2. Existing Work

It is noteworthy that the work presented falls into the more general definition of “ISM,” which according to Skomorohov encompasses any endeavor which takes place outside of the Earth’s atmosphere and which performs any of these three activities: fabrication, assembly, and integration.^[5] ISM concepts include for example the fabrication of large truss structures developed by Tethers Unlimited Inc., contracted by NASA. An overview of advantages and cost feasibility studies of ISM was explored by Trujillo et al.^[6]

Considering the AM of spare parts in space only, since 2016 there exists an AM facility aboard the ISS. In this context, astronauts have produced a number of plastic parts, including spare parts, utilizing a Fused Deposition Modeling (FDM) printer developed by Made in Space Inc., contracted by NASA. This 3D printer works by melting and extruding a polymeric filament through a heated nozzle, similarly to the tools which have nowadays become available for the consumer market. The introduction of the first 3D printer aboard the ISS has been a milestone for the future of AM in space. However, FDM has some limitation on the geometry and materials used (mainly thermoplastic polymers). Since then, in 2006 the Chinese Academy of Sciences tested a similar FDM 3D printer in μ -gravity and recently developed a digital light processing AM technology to produce ceramic green bodies.^[7]

In industrial application, the AM of components from different materials requires the use of different technologies. Moreover, there exists a variety of AM technologies all having particular advantages for manufacturing different types of geometries. Consequently, the adaptation of a range of AM machines would be necessary to produce all kinds of spare parts. On the other hand, for ISM of spare parts neither form nor design are of major concern, but function is. Therefore, a careful selection of two or three of the most powerful AM technologies would suffice. Laser-based AM in particular would enable the fabrication of high-performance metals and thermoplastic polymers in space.

Researchers from the University of Birmingham have tested in 2016 the directed energy deposition of aluminum wire in an European Space Agency (ESA) campaign of parabolic flights. According to the statements of the researchers involved, printed objects would necessarily have to be machined to their final dimensions, as the process used is clearly lacking accuracy compared to powder-based LBM.^[8] The application of powder bed AM in μ -gravity conditions however has not been demonstrated yet. LBM especially is a powder-based AM technology to produce highly complex and high-performance metallic^[9] and thermoplastic^[10] parts with little postprocessing needed. In contrast, DED processes typically need additional machining to reach the desired geometry and surface quality.

In 2010, authors from Made in Space Inc. reviewed AM technologies for an application in μ -gravity conditions and considered LBM as not compatible, due to difficulties of handling powders in the ISS.^[11]

1.3. Aim of this Work

In this manuscript it is shown that recent technological advances could make LBM applicable in μ -g environment and thus making its tremendous success in industrial application accessible for the use in space.

The challenge which the current paper addresses is how to manipulate powder materials in μ -g to deposit stable powder layers.

Depositing powder layers for powder-based AM in absence of gravity is a challenging task, since layer formation is generally governed by gravitational forces:

- 1) Gravitation directs the flow of the powder, allows its homogeneous distribution in form of a layer, and enables a certain degree of compaction.
- 2) Gravitation stabilizes the powder bed and prevents the particles from leaving the building unit. The powder bed should be at least stable against the forces developed during deposition and other forces which may be applied to the powder (e.g., due to vibrations).

2. Experimental Setup

2.1. Powder-Based AM in μ -Gravity: Gas Flow-Assisted Powder Deposition

In this work, a method to stabilize powder layers by establishing a gas flow throughout the powder bed is proposed and has been tested in three DLR's (Deutsches Zentrum für Luft- und Raumfahrt) parabolic flight campaigns. The so-called gas flow-assisted powder deposition is based on a porous building platform acting as a filter for the fixation of metal particles in a gas flow, which is driven by a reduced pressure established by a vacuum pump underneath the platform.

A schematic of the setup used in the zero-g experiments is presented in **Figure 2**.

The gas flow established by means of a vacuum pump throughout the powder bed imposes a drag force on the particles, which in average is directed toward the porous building platform, that is, in the direction in which the gravitational

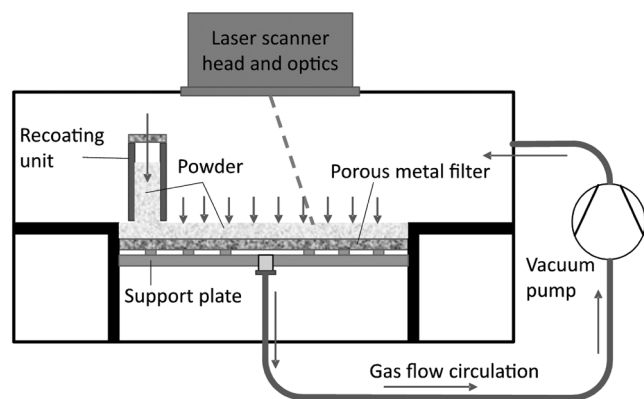


Figure 2. Schematic of the powder deposition unit. The area of the porous building platform for the powder deposition was $106.5 \times 85.5 \text{ mm}^2$.

force would normally act. This force can stabilize the powder bed even when the gravitational force is absent. The porous building platform is not only supporting the powder, but it also acts as a filter to prevent the powder from being dragged into the pump. The vacuum pump is attached via a conventional vacuum hose and a vacuum tight adaptor plate to the porous vacuum base plate.

It is important to notice that the gas circulates in a closed loop and that the atmosphere was carefully controlled at the beginning of the experiment. For stainless steel powder, a nitrogen atmosphere was used. A nitrogen or argon atmosphere is commonly used in commercial LBM equipment to avoid oxidation of the metal powder and to ensure the safety of operation.

During the experiments, the oxygen concentration was $<0.2\%$.

The powder delivery systems used, the so-called recoater, were either roller type with a separate gas flow stabilized reservoir or blade type with a powder box, as illustrated in **Figure 2**. Since the design of the recoater plays an essential role on the reliability of the process, a dedicated paragraph in **Section 4.1** describes the development and testing of this component.

2.2. Parabolic Flight Campaigns

The working principle of the “gas flow-assisted powder deposition”, introduced in **Section 2.1**, was tested in μ -gravity conditions in the course of the 30th, 31st, and 33rd DLR campaigns of parabolic flights, operated by the French company Novespace in Bordeaux. Parabolic flights have the advantage of being the only platform available for experimenters to personally perform tests in μ -gravity conditions.

In a campaign, the experimental setup was mounted aboard an appositely modified Airbus A310. The airplane flies a maneuver which is named “parabola,” consisting of three phases as shown in **Figure 3**. In a first phase, the airplane gradually reaches an inclination up to 47° . In this phase, named “pull-up,” an increased acceleration of 1.8 g (hyper gravity) acts

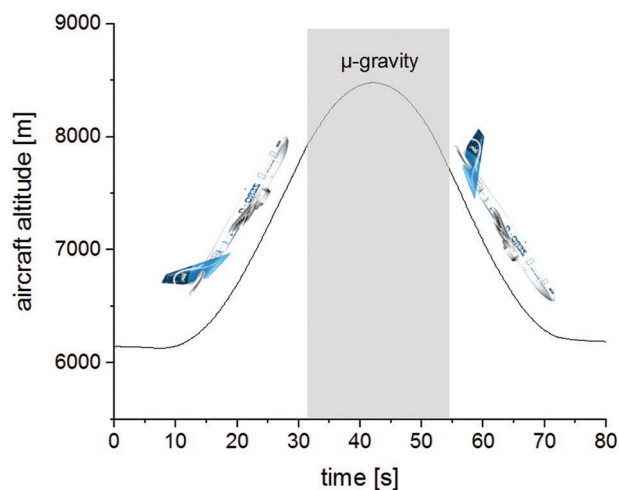


Figure 3. Schematic of an airplane flying a maneuver defined as “parabola.” The airplane image is courtesy of Novespace.

in direction perpendicular to the floor of the airplane. After reaching 47° nose up and flying the cap of the parabola until 42° nose down, 22 s of μ -gravity are experienced. This is followed by again ≈ 1.8 g of “pull-out” at the end of the parabola transferring the steep descent into a horizontally oriented steady flight phase.

Each campaign consisted of three to four flights with 31 parabolas consecutively flown in one flight, summing up to ≈ 34 respectively 45 min of μ -gravity.

As in commercial LBM equipment, also in the “gas flow-assisted powder deposition” parts are manufactured layer by layer. Each built layer consists of

Step 1) deposition of a thin powder layer

Step 2) inscribing the respective layer information by selectively laser melting the powder.

One layer (100 μ m thick) was deposited in the μ -gravity phase of each of the 31 parabolas, resulting in a maximum height of the parts of 3.1 mm. Since the 22 s at μ -g were not sufficient to complete both process steps, layer deposition and laser melting had to be performed in different stages of the parabolic flight.

The primary objective of this work was to prove the feasibility of depositing and stabilizing powder layers at μ -gravity by the “gas flow-assisted powder deposition” process. For this study, experiment configuration A (Figure 4 a) was implemented: the powder deposition was performed in the 22 s μ -g phase, followed by laser melting in the successive steady flight phase.

In addition, 1 day of the 31st campaign was dedicated to study the effect of different acceleration conditions in the laser melting step. For this study, the experiment configuration B in Figure 4b was implemented: the powder deposition was performed in the 1 g steady flight phase before the parabola. Successively, one set of samples was laser melted in the μ -g phase, followed (in the same layer) by one set of samples laser melted in the 1.8 g hyper gravity phase and finally by one set at 1 g.

2.3. Gas Flow-Assisted Powder Deposition Setup for Parabolic Flights

This section describes the main components which differ from a standard LBM equipment and had to be designed specifically for the experiments aboard the parabolic flights.

The custom setup built for the experiments consisted of two racks, as shown in Figure 5.

The powder deposition unit and the laser system, which includes the laser module, scanner, and optics are mounted on rack 1. This unit includes the actual LBM system.

The gas circulation pump, the electrical cabinet, and the computers for controlling all operations of the LBM system, that is, layer deposition and laser, are mounted on rack 2.

Rack 1 had a dimension of 800 \times 800 \times 1000 mm³ and a weight of 188 kg, while rack 2 had a dimension of 800 \times 600 \times 500 mm³ and a weight of 146 kg. The maximal power consumption amounts to about 1.2 kW.

It can be evinced that the racks were substantially lighter than standard commercial LBM equipment, despite fulfilling all additional requirements related to flight safety. For comparison,

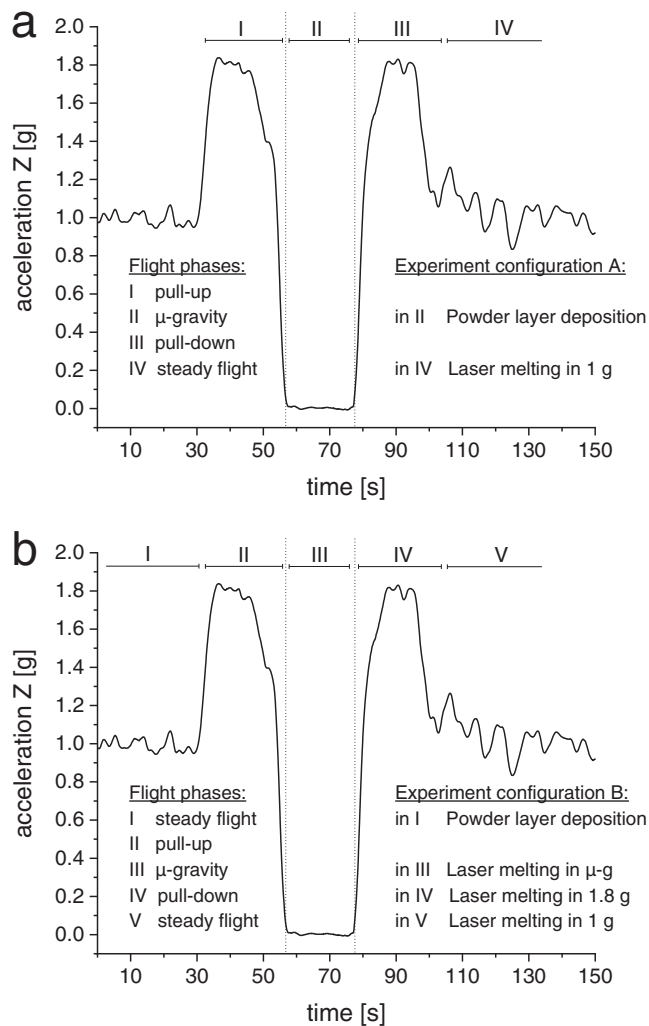


Figure 4. a) Experiment configuration A to test the powder deposition in μ -g conditions. b) Experimental configuration B to test the laser melting at μ -g, 1 g, and 1.8 g conditions, respectively.

most small commercial LBM machines weigh in the range of 500–1300 kg and have a power consumption of 1.7–3 kW.

Concerning the processing of powders in the airplane, the system was designed to have a double containment at all time. The major requirement for the mechanical design was that the racks must sustain their load up to an acceleration of 9 g along the long axis of the airplane cabin, in case of emergency landing. For an application in space, it has to be noted that the design can (and must) be further reduced in size and weight.

The entire system flooded with process gas, including hoses, flowmeter, valves, and pump, was designed in a gas tight fashion and provides a double containment against leakage of powder. Technologically challenging was the design as vacuum tight system, up to 10⁻⁴ mbar, which can withstand an internal overpressure of 1.5 bar relative to the outer atmosphere and which can be operated completely independent of the outer atmosphere pressure. From start to flight and landing the pressure in the airplane varies typically between 0.85 bar and normal pressure (≈ 1.013 bar). Moreover, in case of cabin depressurization,

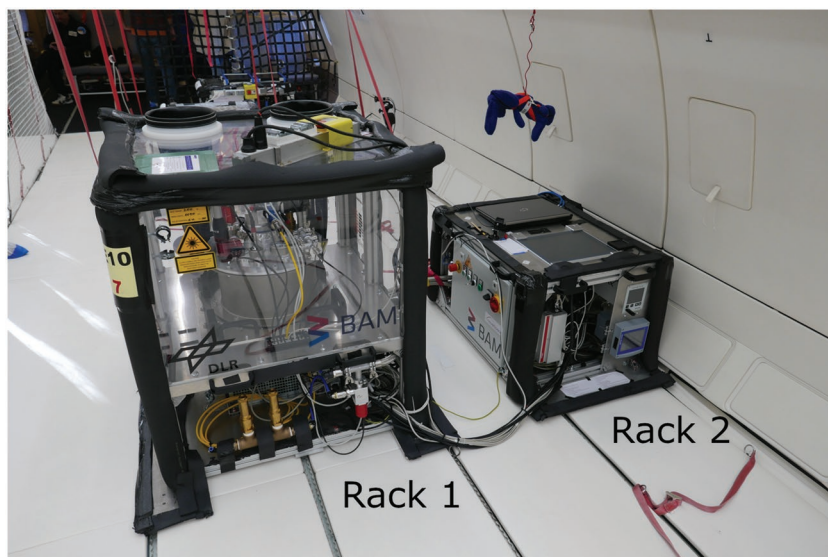


Figure 5. Photo of the setup for LBM in μ -gravity mounted in the Airbus A310 ZERO-G during the 33rd DLR parabolic flight campaign. Rack 1 contains the laser system and the deposition unit while rack 2 comprises the gas circulation pump and the control system.

the pressure in the airplane might drop rapidly to 0.35 bar. After purging the laser chamber and filling it with the process gas, the gas was circulated for the duration of the flight. Circulation of the process gas was maintained by a scroll type vacuum pump, considering that oil pumps are not allowed in the airplane. The pump generated a reduced pressure at one side of the porous building platform, thus drawing the gas through the platform and the powder deposited thereon. The same pump served for evacuation

of the system before purging with nitrogen. The vacuum pump was protected against contamination by powder with an Atmosphères Explosibles (ATEX) certified vacuum filter. The building platform, $106.5 \times 85.5 \text{ mm}^2$ in size, was machined from a 5 mm thick sinter metal plate (stainless steel AISI 316L/B) with a filter grade efficiency of $9 \mu\text{m}$.

3. Results

3.1. Laser Beam Melting in μ -Gravity

A 12 mm wrench was chosen as a demonstrator for proving the feasibility of the LBM process in μ -g. The wrench with handle has a length of $\approx 55 \text{ mm}$ and has a light-weight design. **Figure 6a** shows a top view of the LBM process chamber containing the powder deposition unit. Mounted on the top of the chamber are the laser scanner and collimator, three pressure gauges and two overpressure valves.

Figure 6b shows the powder bed, after partially removing the powder, deposited in μ -gravity during 31 parabolas and the two laser melted wrenches embedded. The same samples are shown in **Figure 6c** on the porous metal plate after cleaning. The “ZERO-G” wrench is shown in **Figure 6d** after its separation from the base plate.

These samples are the first metal parts ever 3D printed in μ -gravity by LBM. The building strategy corresponds to

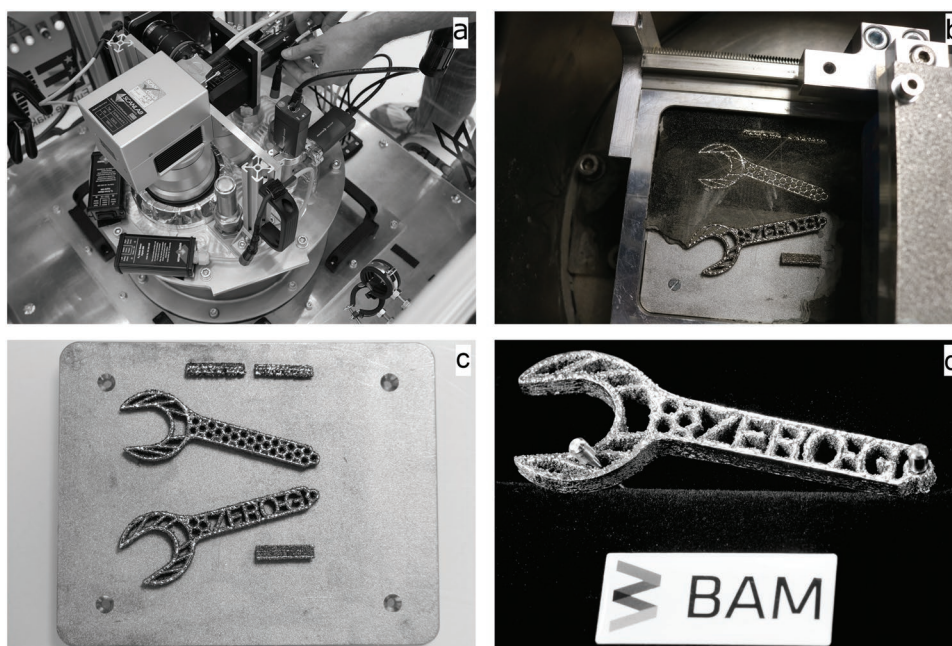


Figure 6. a) Top view of the deposition chamber, showing the laser scanner and optics, two oxygen sensors, two pressure gauges, and two overpressure safety valves b) view of the deposition unit during cleaning after a parabolic flight, showing the wrenches produced by LBM still partially embedded in the powder bed c) top view of the porous metal base plate and of the wrenches manufactured in μ -gravity d) 12 mm wrench manufactured in μ -gravity, after separation from the base plate. The base plate has a size of $106.5 \times 85.5 \text{ mm}^2$.

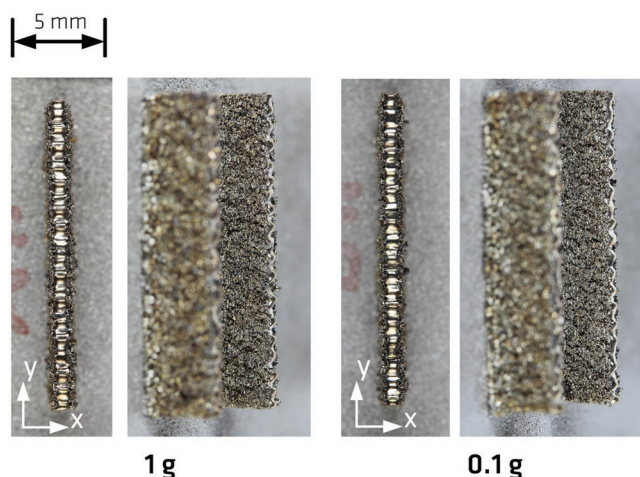


Figure 7. Specimens manufactured in different g conditions, top view, and inclined side-view; left: 1 g ; right: μ - g .

experiment configuration A illustrated in Figure 4a, that is, layer deposition at μ - g followed by laser melting during steady flight at normal g . It was assumed that laser melting can be performed independently from the acceleration applied. Certainly, this general viewpoint is only valid as long as it concerns the feasibility of the process. For studying the influence of the acceleration on the microstructure of the parts manufactured, the experiment configuration B illustrated in Figure 4b has been chosen.

One of the demonstrator parts manufactured with the powder deposited at μ - g was scanned by X-ray micro-computed tomography. An animation of the 3D reconstruction based on the scan is available in the Video S1 in the Supporting Information. No defect structures which could be associated to μ - g conditions are noticeable.

From a macroscopic point of view, no significant differences between the thin-walled specimens manufactured in μ - g

conditions compared to those manufactured in 1 g condition can be noticed, as it can be seen in Figure 7.

Optical images of cross sections indicate solid material in the inner wall area and sintered powder at the side surfaces (Figure 8). Due to the very low hatch distance of scanning vectors and the double melting strategy, measuring of melt pool geometries is not possible at the cross sections. However, the cross sections clearly reveal a complete melting in the inner of the wall with very low incidence of porosity or other defects at the specimen produced in μ - g conditions (Figure 8).

Electron backscatter diffraction (EBSD) generally revealed a microstructure typical for LBM processed stainless steel 316L. Exemplarily, Figure 9 illustrates the grain distribution (minimal misorientation angle: 5°) in a μ - g specimen.

Caused by the small dimension of the wall compared to the size of formed and solidified droplets, and the various grain size, form, and shape, the microstructure can be characterized as very complex. The applied target preparation finally decides about the investigated section plane through an extremely diverse microstructure. Therefore, any extraction of statistically significant microstructure characteristics appears at least challenging. Despite these adverse circumstances, cross as well as longitudinal section proves the formation of elongated grains with increasing distance to the wall surface. For the applied processing regime, grains grow over several layers. The grain coarsening is controlled by growth competition of differently oriented grains. The inclination of the growth axis is very likely the result of the applied scanning velocity and the resulting heat transfer (solidification front). Detailed results about the influence of different accelerations on the microstructure of the material are not the aim of the present work and will need dedicated further work.

3.2. Gas Flow through the Powder Bed

It was found that for the present setup, that is, $106.5 \times 85.5 \text{ mm}^2$ base plate, a gas flow of $10\text{--}20 \text{ L min}^{-1}$ was necessary to

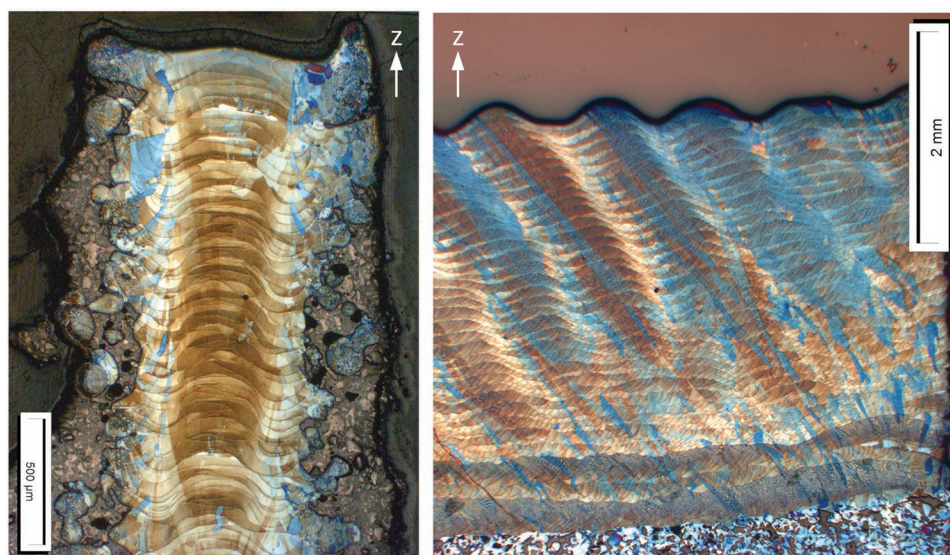


Figure 8. Light microscopy of thin-walled specimen manufactured in μ - g condition; left: front face view; right: side face view.

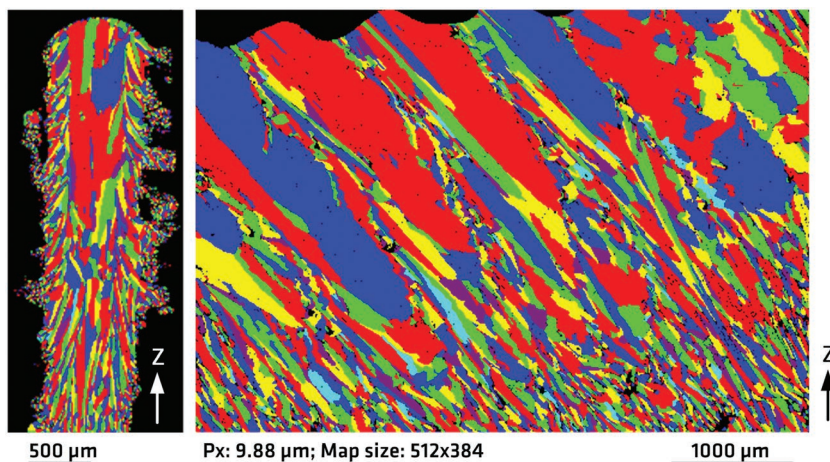


Figure 9. EBSD grain distribution mapping of a μ -g specimen, left: front face view; right: side face view.

stabilize the powder deposition and the powder beds. A flow higher than 20 L min^{-1} caused rough layers with an inhomogeneous surface.

Figure 10a reveals a measurement of the gas flow throughout the central area of the base plate (28 cm^2) and powder deposited thereon as a function of the powder bed thickness, with each layer deposited 0.1 mm thick.

The pressure drop through the powder bed was calculated after removing the contribution of the pressure drop through the other elements between the powder and the pump (porous metal plate, filters, tubing, etc.).

The gas velocity through the powder bed, u , was calculated by dividing the volumetric gas flow Q by the section area A , considering a porosity $\varepsilon = 0.5$ estimated from the bulk density of the powder.

According to Darcy's law

$$u = -\frac{K}{\mu} \frac{\Delta P}{L} \quad (1)$$

where K is the permeability of the powder bed ($[K] = \text{m}^2$), μ is the dynamic viscosity of the gas, and L is the thickness of the powder bed.

Rearranging Equation (1) and plotting $\Delta P/u$ as a function of L results in a straight line with slope μ/K . Interpolating the experimental data as in **Figure 10b** resulted in a permeability $K = 4.22 \cdot 10^{-12} \text{ m}^2$.

Estimating the permeability of the powder bed by the Carman-Kozeny equation, considering the diameter of the particles as $D_{50} = 37 \mu\text{m}$ and $\varepsilon = 0.5$, resulted in $K = 3.80 \cdot 10^{-12} \text{ m}^2$, which is in reasonable agreement with the permeability calculated from the experimental measurements.

From the experimental value of permeability, it can also be estimated that if the maximum $\Delta P = 1013 \text{ mbar}$ was available, then (for an area of 28 cm^2) a minimum gas flow of 20 L min^{-1} could be maintained up to a powder bed thickness of 80 mm . It could still be possible to stabilize thicker powder beds by increasing the pressure on the top side of the building chamber, resulting in a pressure drop across the powder bed larger than 1 bar .

4. Discussion

4.1. Recoater Design for the Deposition of Powder Layers at μ -Gravity

Over the course of the three campaigns of parabolic flights, it was shown that the gas-assisted powder deposition setup was able to stabilize a powder bed in μ -g conditions. Noticeably, once the powder bed is formed, the particles are hindered from detaching from the surface. This is intuitively understandable: since the acceleration which acts on the powder is in all directions in the μ -g range (typically below 0.01 g), even a small gas flow can effectively stabilize the powder bed.

The situation is different for the powder which forms a new layer during the recoating

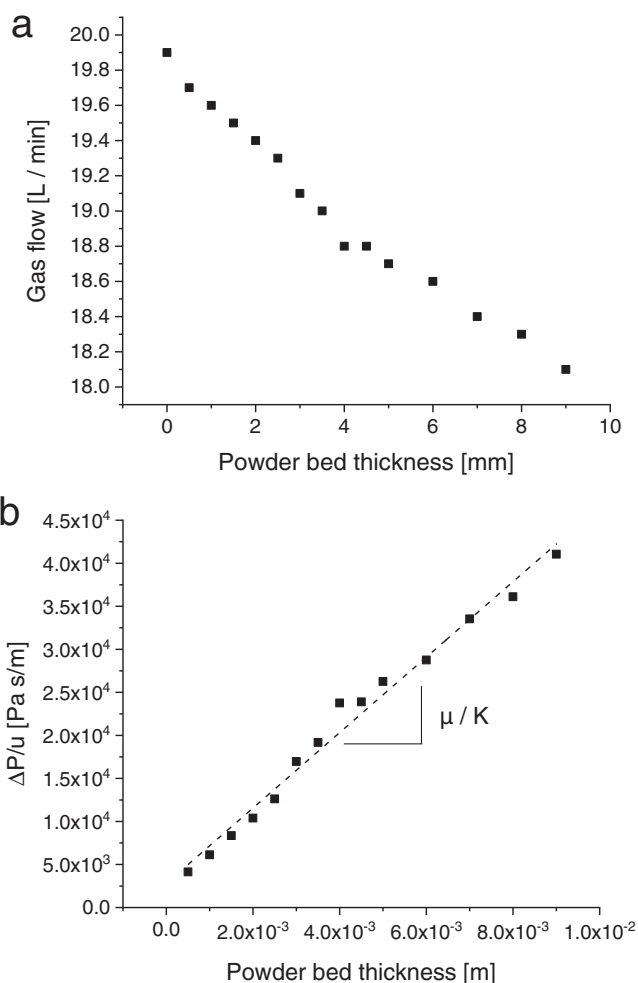


Figure 10. a) Measured gas flow through the powder bed as a function of the powder bed thickness. The pressure difference for maintaining the gas flow was in the range of 950 mbar and the area of the powder bed was $\approx 28 \text{ cm}^2$. b) $\Delta P/u$ as a function of the powder bed thickness. ΔP is the pressure difference through the powder bed in Pa, u is the gas velocity in m s^{-1} .

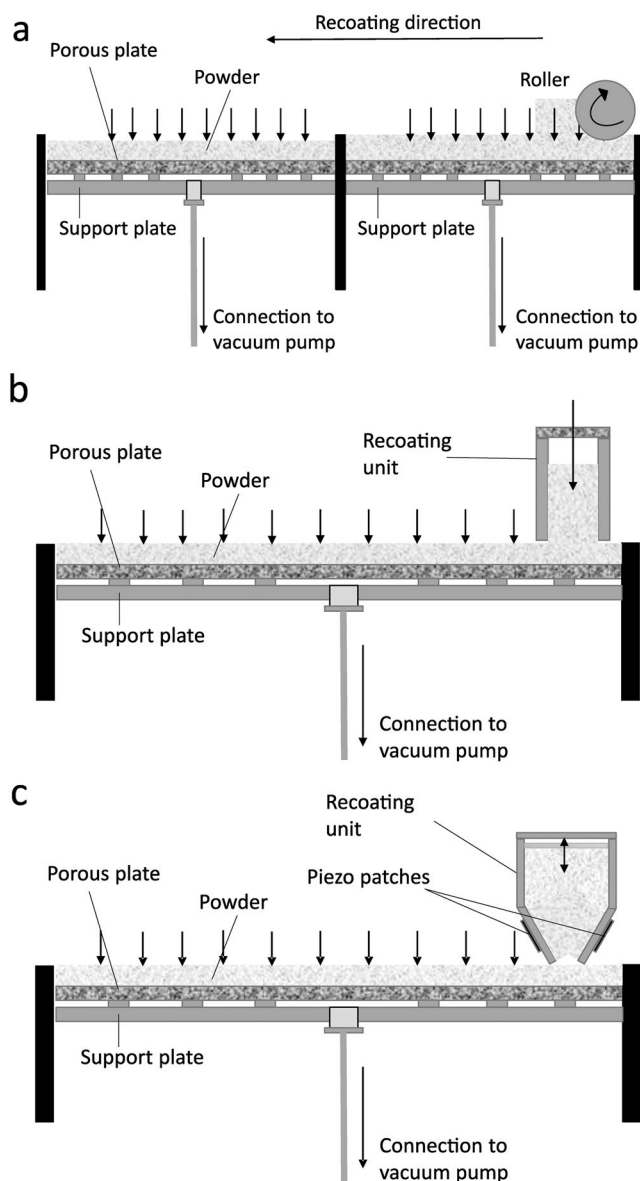


Figure 11. Schematics of the three different recoater designs tested: a) roller; b) box type double blade; c) V-shaped with piezo activation.

step, because the recoater while moving activates the flow of the powder to homogeneously distribute it.

The design of the recoater therefore is critical both to

- 1) homogeneously feed the powder on the full width of the layer
- 2) initiate the flow and spread the powder, but without causing the lift-off of the particles from the powder bed.

In the first series of experiments, in the 30th DLR campaign, a roller recoater was tested, designed according to the schematic shown in **Figure 11a**. This type of recoater can feed the powder homogeneously over the width of the plate, but on the other hand, it makes difficult to reproducibly activate the flow of powder in a controlled way, depending on the quality of μ -gravity which is different in every parabola. This effect is clearly shown in Videos S2 and S3 in the Supporting

Information. Video S2 in the Supporting Information shows a homogeneous layer deposition in μ -gravity, while Video S3 in the Supporting Information shows another layer, in which the powder in front of the recoater lifts off. It is noteworthy that the powder used in this first campaign was a ceramic powder, i.e., silicon carbide (SiC), simply for demonstration of all major functionalities of the LBM machine and its safe operation, without imposing any risk by potentially explosive, electrically conductive and harmful steel powders.

The deposition unit used in the 31st DLR campaign (see **Figure 11b**) consists of a box moving on top of the powder bed with two parallel edges. During layer deposition, the leading edge of the box has no function other than preventing the powder from flowing out of the box, while the trailing edge defines the layer thickness. This setup is designed for preventing a complete lift-off of the particles, since the powder is always enclosed in the box. For establishing a steady gas flow throughout the powder reservoir, thus, attracting the powder toward the surface of the powder bed, the box had a lid made of a metal filter. However, in μ -gravity it was found that the powder had the tendency to aggregate inside the recoater and not flow homogeneously to cover a full layer in a reproducible manner.

The design implemented in the 33rd DLR campaign so far produced the most reproducible layer deposition. It is an evolution of the precedent recoater, based on the schematic shown in **Figure 11c**. An example of deposition of a powder layer in μ -gravity is shown in Video S3 in the Supporting Information.

In this design, the powder is contained in a reservoir which is V-shaped at the bottom and ends with a thin slit (1 mm). At the top, the powder is slightly compressed by a mechanism to avoid the free-floating and aggregation of the powder at one side of the recoater. In between individual layer deposition events, while the recoater is standing still on top of the powder bed, the powder does not flow through the thin slit. The powder flow can however be activated in a controlled way for the layer deposition by a high-frequency vibration induced by a piezo actuator. This switchable powder flow appears promising for a reproducible layer deposition with minimum loss of powder in μ -g. The design of the recoating unit has been found to be essential to control the powder deposition and further optimization will be necessary to achieve a fully independent and reliable production.

4.2. Stabilization of Powder Layers at μ -Gravity

The stabilization effect of the powder in μ -gravity can be understood by considering the magnitude of the forces acting on the particles in the powder bed.

Without a gas flow, two main forces act on each particle: F_g = gravitational force, F_{pp} = sum of the interparticle forces between a particle and its neighbors. The flow and packing of a powder is controlled by the interplay of these two forces.

For a particle of radius R

$$F_g = \rho \cdot V \cdot g \quad (2)$$

where ρ is the density of the particle, $V = 4/3\pi R^3$ its volume, R its radius, and g the gravitational acceleration.

Table 1. Drag force F_d and gravitational force F_g compared for stainless steel spheres at different acceleration values and for different particle sizes.

Particle diameter [μm]	F_d for $u = 0.118 \text{ m s}^{-1}$ [N]	F_g at 1 g [N]	F_g at 0.01 g [N]
1	1.97×10^{-11}	4.02×10^{-14}	4.02×10^{-16}
10	1.97×10^{-10}	4.02×10^{-11}	4.02×10^{-13}
38	7.50×10^{-10}	2.22×10^{-9}	2.22×10^{-11}
100	1.97×10^{-9}	4.02×10^{-8}	4.02×10^{-10}

F_{pp} strongly depends on the size, shape, and roughness of the particles, the distance between them and the presence of adsorbed layers or existing surface charges. In a flowable powder typically F_{pp} is in the order of magnitude of F_g or lower.

In absence of gravitational forces, the interparticle forces dominate the flow behavior of the powder, making challenging to define a flow direction to form homogeneous layers. Even when the particle surfaces would be functionalized for deliberately tuning the interparticle forces, it appears extremely difficult to impossible finding an interparticle interaction potential allowing, on one hand, a satisfactory particle packing density and, on the other, preventing an agglomeration of particles and, thus, allowing a deposition of smooth densely packed layers.

In the “gas flow-assisted powder deposition”, due to the gas flow, an additional force F_d (drag force) acts on the particles. In the following section, it is estimated in which conditions the magnitude of this force F_d is relevant compared to F_g (in 1 g).

The drag force F_d can be calculated if the flow field is known. In our setup, the air flow has a velocity whose average direction is parallel to F_g , and amounts to $u = 0.118 \text{ m s}^{-1}$, according to Equation (1) with $A = 106.5 \times 85.5 \text{ mm}^2$ and $Q = 20 \text{ L min}^{-1}$.

Considering a particle on top of the powder bed, in these conditions it is possible to calculate the Reynolds number, which results in $Re \approx 0.3$ for particles with a diameter of $38 \mu\text{m}$. This diameter was chosen for this estimation since it corresponds to the D50 of the particle size distribution of the stainless steel powder used in this work.

For small Reynold numbers (<1), the Stokes equation can be used to calculate approximately the drag force

$$F_d = 6\pi\mu Ru \quad (3)$$

Using Equations (2) and (3) to calculate F_g and F_d for spherical stainless steel particles ($\rho = 7890 \text{ kg m}^{-3}$), gives the results reported in **Table 1**.

This qualitative calculation supports the viewpoint, that the gas flow results in drag forces which not only are significant, but they are of the same order of magnitude than gravitational forces in μg conditions ($<0.01 \text{ g}$) for particles with a diameter of $38 \mu\text{m}$ and even much higher for fine powders $<10 \mu\text{m}$. These theoretical considerations are in full agreement with the observation, that a powder deposition and stabilization in the powder bed at $\mu\text{-g}$ was possible. The conditions in a parabolic flight at $\mu\text{-g}$ are even more challenging than in space. Generally, the acceleration in all three coordinates x , y , and z is below 0.01 g . However, the acceleration can act in both directions, which is, plus and minus z . Therefore, there is always the chance that it is acting exactly against the drag forces provided by the gas flow. In space, the $\mu\text{-g}$ quality is significantly better, and the

flow rate of the gas could be much smaller for a safe stabilization of the powder bed. This fact is important when considering the need of reducing the weight of the equipment, since the vacuum pump contributes significantly to the total payload.

It is interesting to notice that the application of a gas flow during the powder deposition can influence the density of the powder bed. This effect has been described by Zocca et al. for ceramic and glass powder, showing that the packing density significantly increased with the application of a gas flow, but that the magnitude of the increase greatly depended on the powder used.^[12] Further studies are being carried out also with other powder materials.

A complete study of the packing density during the parabolic flights has not been possible, given the technical complexity and limited $\mu\text{-gravity}$ time. It is also not clear if parabolic flights are a suitable platform for testing variations in powder bed density, because during the flight the acceleration conditions vary between $\mu\text{-gravity}$ and 1.8 g , and rearrangements of the powder cannot be excluded. However, this aspect will be important for a further qualification of the process, since the packing density of the powder bed can influence the quality of the parts produced by LBM.

Regarding the gas flow, one additional point deserves a more detailed discussion: the manufacture of dense parts. In case a structure has completely dense large areas, a gas flow cannot be established over the cross section of this part, making the stabilization of layers on top of such a structure in $\mu\text{-g}$ impossible. The gas flow can however bridge thin walls or struts even if the material is dense. In the sequence of experiments performed, a wall thickness of 2 mm was not critical, see the printed wrench in Figure 6. At higher wall thicknesses the stabilization of freshly deposited powder became increasingly difficult and survival of a layer became dependent of the quality of each individual parabola. In this context it is noteworthy that the deposit of smooth layers was generally no problem, but stabilization of the layers was critical at wall thicknesses larger than 2 mm . Hence, it can be assumed that the buildup of structures with dense features even larger than 2 mm would be possible at better $\mu\text{-g}$ quality. Moreover, lightweight design generally does not rely on voluminous dense parts and for saving material many structures will be composed out of more or less filigree features ideally for applying the “gas flow-assisted powder deposition.”

4.3. Laser Beam Melting in $\mu\text{-Gravity}$

The wrench shown in Figure 6 was manufactured by depositing powder in $\mu\text{-gravity}$ and by laser melting during the steady flight (procedure illustrated in Figure 4a); therefore, no significant difference in the material microstructure was expected between this part and the same print job reproduced on ground.

Samples in the form of thin free-standing walls (1 mm thick) were manufactured by depositing powder in steady flight and by laser melting in $\mu\text{-gravity}$ (procedure illustrated in Figure 4b). These samples had an appearance and a density comparable to the wrench shown in Figure 6, suggesting that an LBM process could be fully performed in $\mu\text{-gravity}$ producing dense components.

It is known that the microstructure of 316L stainless steel manufactured by LBM is generally complex, with features ranging from hundreds of μm (grains) down to precipitates and impurities in the submicron and nanometer range.^[13] The material processed by LBM is generally composed of γ (fcc) austenite with a small fraction of δ (bcc) ferrite, which is influenced by the laser parameters used.^[14]

Given the small size and the limited number of samples available in this work, a complete microstructural analysis has not been possible. EBSD analysis revealed the presence of a columnar structure with elongated grains (Figure 9), which is often observed in the LBM of stainless steel 316L.^[14] However, the growth axis of these elongated grains is inclined against the build direction by about 40° . This can most likely be attributed to the heat transfer conditions resulting from the applied scanning strategy. Importantly, the microstructure is strongly influenced by the laser parameters and even in a single sample can vary depending on the position. In general terms, the solidification of the material is controlled by the ratio temperature gradient/growth rate and the ratio solidification undercooling/diffusion coefficient. In particular, for a decreasing ratio temperature gradient/growth rate, a planar, columnar, or equiaxed dendritic structure is expected.^[15]

The major phenomena affecting the formation of a melt pool during laser scanning are driven by surface tension, capillary forces and inertia effects, while viscous and gravity forces can be considered as secondary effects.^[16] For this reason, parts fabricated by LBM in μ -gravity are not expected to be significantly different compared to parts fabricated by LBM in 1 g.

Additionally, as described by Meier et al. and by Khairallah et al., while the heat transfer within the melt pool is governed by convection rather than by heat conduction, Marangoni convection (driven by surface tension gradients) plays a prominent role rather than gravitational (buoyancy) convection.^[17]

However, when the laser process is conducted in the so-called keyhole mode, the laser locally vaporizes the melt pool surface and produces a keyhole, into which the laser beam radiates deeper into the material leading to significantly deeper melt pools. The keyhole shape and thus also the resulting molten pool geometry is determined by an equilibrium of forces between evaporation pressure (recoil pressure), surface tension (Laplace pressure), and the static pressure of the metallic liquid. In zero gravity conditions, it can therefore be assumed that the melt pool geometry will change slightly due to the elimination of the static pressure.

For this reason, the density and microstructure are not expected to be majorly affected by LBM in a μ -gravity environment. Small differences at the microstructural scale however cannot be excluded and are going to be object of dedicated future analysis.

5. Conclusions

A stainless steel metal powder has been successfully processed in the LBM process at microgravity (μ -g) conditions in a parabolic flight campaign. For compensating the forces typically provided by gravitation, a gas flow has been established throughout the powder bed. It could be shown, that

the drag forces provided by the gas flow are comparable or even exceeding the forces acting on the particles in μ -g acceleration conditions (<0.01 g) for particles with a diameter of $38 \mu\text{m}$ (which is the D50 of the powder used in this work). In this study, the worldwide first metallic tool, a 12 mm wrench has been manufactured by LBM at μ -g conditions. Moreover, other parts have been manufactured at different accelerations provided by a parabolic flight, that is, hyper gravity (1.8 g), μ -g (<0.01 g), and 1 g. In a first survey of the parts microstructure, no significant deviations from a part manufactured at 1 g conditions have been found. Hence, the current work has presented the first results on the feasibility of an LBM process for additively manufactured ready to use metal parts in space.

6. Experimental Section

Materials: In principle, the gas flow-assisted powder deposition could be applied to any ceramic, metallic, or polymeric powder suitable for the deposition of thin layers.

The material of choice for the experiments described in this manuscript was a commercial 316L stainless steel powder (SLM Solutions GmbH, Lübeck, Germany) with an apparent packing density of 3.97 g cm^{-3} , according to supplier's specification, and a particle size distribution described by the intercepts of the cumulative mass D10 of $23.77 \mu\text{m}$, D50 of $37.65 \mu\text{m}$, and D90 of $62.62 \mu\text{m}$.

Components for the Gas Flow-Assisted Powder Deposition Setup: The vacuum pump used was a scroll type pump with a nominal flow rate of $30 \text{ m}^3 \text{ h}^{-1}$ (ScrollVac SC-30-D, Leybold GmbH, Germany).

An ATEX Filter (CLS series, Solberg Manufacturing Inc., IL, USA) was implemented as protection of the pump from particle contamination. Additional filters (Novacom FIL L 38) were used both after the building platform and before the inlet of the gas into the building chamber.

For the building platform, 5 mm thick sinter metal filter made of stainless steel (AISI 316L/B) and with a grade efficiency according to ASTM F 795 of $9 \mu\text{m}$ ($T = 98\%$ absolute) were purchased from GKN Sinter Metals Filters GmbH, Germany. The building platforms were directly cut from the plates without further machining.

Laser Parameters and Process Atmosphere: For fusing the metal powder in the LBM process an IPG (IPG LASER GmbH, Burbach, Germany) 200 W cw. fiber laser emitting at a wavelength of 1070 nm and a ScanLab (ScanLab GmbH, Puchheim, Germany) laser optics have been employed. The spot size of the laser on the powder surface was $\approx 48 \mu\text{m}$. In the LBM experiments the laser was operated at an average power output between 100 and 120 W.

The stainless steel wrenches, shown in Figure 6, were produced as a demonstrator with the following parameters:

Layer thickness = 0.1 mm

First scan: laser power = 100 W; scan velocity = 500 mm s^{-1} ; hatch distance = 0.024 mm.

Second scan: laser power = 120 W; scan velocity = 500 mm s^{-1} ; hatch distance = 0.024 mm.

The walls produced in different acceleration conditions, shown in Figure 7, were produced with the following parameters:

Layer thickness = 0.1 mm

Scanned twice: laser power = 120 W; scan velocity = 500 mm s^{-1} ; hatch distance = 0.024 mm.

The hatching of the walls was performed with vectors perpendicular to the long side of the wall.

The laser melting experiments were carried out in nitrogen atmosphere. A nitrogen or argon atmosphere is commonly used in commercial LBM equipment to avoid oxidation of the metal powder and to ensure the safety of operation.

To ensure the purity of the atmosphere, the inner chamber of the LBM machine was evacuated and back filled with nitrogen for 3–4 cycles, until reaching an oxygen concentration below 0.2 vol%, (measured by

two oxygen sensors, Mettler Toledo, USA) at an absolute pressure of 850 mbar (measured by two pressure sensors, Pfeiffer Vacuum GmbH, Germany).

Macro- and Microstructure Analysis: Sections of the thin-walled samples were polished and etched with Beraha II solution before analysis under an optical microscope and scanning electron microscope.

Electron backscatter diffraction (EBSD) investigations were performed at 20 kV in the scanning electron microscope (LEO 1530VP, Zeiss).

Supporting Information

Supporting Information is available from the Wiley Online Library or from the author.

Conflict of Interest

The authors declare no conflict of interest.

Keywords

3D printing, additive manufacturing, laser-beam melting, micro gravity

Received: June 14, 2019

Revised: July 31, 2019

Published online:

-
- [1] NASA, Audit Report IG-02-011, **2002**.
[2] D. Culpan, <https://www.wired.co.uk/article/iss-supplies> (accessed: June 2019).
[3] T. Malik, <https://www.space.com/7088-tool-bag-lost-space-meets-fiery.html> (accessed: June 2019).

- [4] T. DeRoy, H. Wei, J. Zuback, T. Mukherjee, J. Elmer, J. Milewski, A. M. Beese, A. Wilson-Heid, A. De, W. Zhang, *Prog. Mater. Sci.* **2018**, 92, 112.
[5] R. Skomorohov, C. Welch, A. Hein, *67th Int. Astronautical Congress (IAC)*, Guadalajara, Mexico **2016**.
[6] A. E. Trujillo, M. T. Moraguez, A. Owens, S. I. Wald, O. De Weck, in *AIAA SPACE and Astronautics Forum and Exposition*, American Institute of Aeronautics and Astronautics (AIAA) **2017**.
[7] <http://www.3ders.org/articles/20180621-china-pioneers-ceramic-3d-printing-in-microgravity-using-dlp-technology.html> (accessed: June 2019).
[8] M. Molitch-Hou, <https://www.engineering.com/3DPrinting/3DPrintingArticles/ArticleID/13879/Researchers-3D-Print-Metal-in-Zero-G-for-ESA.aspx> (accessed: June 2019).
[9] C. Y. Yap, C. K. Chua, Z. L. Dong, Z. H. Liu, D. Q. Zhang, L. E. Loh, S. L. Sing, *Appl. Phys. Rev.* **2015**, 2, 041101-1.
[10] M. Schmid, K. Wegener, *Proc. Eng.* **2016**, 149, 457.
[11] J. J. Dunn, N. D. Hutchison, A. M. Kemmer, A. Z. Ellsworth, M. Snyder, W. B. White, B. R. Blair, *Space Manufacturing 14: Critical Technologies for Space Settlement*, NASA Ames Conference Center in Mountain View, CA **2010**.
[12] A. Zocca, C. M. Gomes, T. Mühler, J. Günster, *Adv. Mech. Eng.* **2014**, 6, 491581.
[13] Y. M. Wang, T. Voisin, J. T. McKeown, J. Ye, N. P. Calta, Z. Li, Z. Zeng, Y. Zhang, W. Chen, T. T. Roehling, *Nat. Mater.* **2018**, 17, 63.
[14] T. Kurzynowski, K. Gruber, W. Stopyra, B. Kuźnicka, E. Chlebus, *Mater. Sci. Eng., A* **2018**, 718, 64.
[15] K. Saeidi, X. Gao, Y. Zhong, Z. J. Shen, *Mater. Sci. Eng., A* **2015**, 625, 221.
[16] a) C. Meier, R. W. Penny, Y. Zou, J. S. Gibbs, A. J. Hart, *Annu. Rev. Heat Transfer* **2017**, 20, 241; b) C. Körner, A. Bauereiß, E. Attar, *Modelling Simulation Mater. Sci. Eng.* **2013**, 21, 085011.
[17] S. A. Khairallah, A. T. Anderson, A. Rubenchik, W. E. King, *Acta Mater.* **2016**, 108, 36.